ORIGINAL ARTICLE

Fast M_W estimation of microearthquakes recorded around the underground gas storage in the Montello-Collalto area (Southeastern Alps, Italy)

Alessandra Lanzoni · Luca Moratto ⓘ ·
Enrico Priolo · Maria Adelaide Romano

Abstract Underground fluid injection and extraction is able to change pore fluid pressure at depth and make faults unstable, due to friction-force reduction, with an increased possibility of triggering earthquakes. Studying the local seismicity, down to microearthquakes, and stress field in areas where such activities are developed are essential steps to discriminate between natural and induced events. In this context, the moment magnitude (M_W) is a key-parameter to both evaluate the energy balance and the stress involved in earthquake rupture process and assess seismic hazard accurately. Here, we focus on the fast M_W estimation of microearthquakes recorded around the underground gas storage of Collalto (Northeastern Italy) by a dedicated seismic monitoring network. The area of Montello-Collalto, where this industrial activity is carried out, is densely populated and characterized by relevant seismic hazard. We compute M_W from the response spectra (SA) calculated at fixed periods (i.e., 1.0 and 0.3 s); we show that log (SA) and M_W scale as 2/3 and extend our method to microseismicity by using response spectra at 0.1 s. We eventually estimate M_W for 1659 events ($0.4 \leq M_W \leq 3.5$) and find that M_L and M_W scale as 2/3 too. The discrepancy between these two magnitude scales affects both the Gutenberg-Richter parameters and completeness magnitude estimations; therefore, it has consequences when those quantities are used for physical interpretation. Our procedure shows to be efficient and suitable to be implemented within standard routine analyses of real-time monitoring and feed decision-making processes about plant management, such as the traffic light protocols.

1 Introduction

The estimation of the moment magnitude M_W and the related seismic moment M_0 (Hanks and Kanamori 1979) is a fundamental task for investigating the dynamics of the earthquake source process, as M_0 is directly associated with the fault rupture area and, indirectly, to the forces that cause it. At the same time, M_W is preferred to M_L in the probabilistic seismic hazard assessments, both for natural and induced earthquakes. Indeed, unlike M_L, M_W is not affected by saturation, anelastic attenuation, or scattering problems, and therefore, the fault to rupture provides more reliable estimations of the Gutenberg-Richter parameters (a and b values) (Edwards 2015; Staudenmaier et al. 2018).

According to well-established seismological practices, real-time estimations of M_W are obtained from moment tensor solutions that are computed through

A. Lanzoni · L. Moratto (✉) · E. Priolo · M. A. Romano
Istituto Nazionale di Oceanografia e di Geofisica Sperimentale - OGS, Trieste, Italy
e-mail: lmoratto@inogs.it

A. Lanzoni
Università di Trieste, Trieste, Italy

the inversion of long-period waveforms (Dziewonski et al. 1981; Sipkin 1982; Dreger 2002). However, these approaches are effective only in case of strong earthquakes (approximately M > 4) since signals are inverted in the low frequency range (i.e., for periods greater than 10 s). For weaker events, M_W is generally estimated by M_0 obtained from the plateau at the low-frequency spectral band, provided that some basic spectral corrections related to source, wave propagation path, and possible site effects are properly applied (e.g., Abercrombie 2015; Zollo et al. 2014). Of course, this approach requires that the background noise does not dominate the signal in the frequency range corresponding to the plateau, which extends towards the high-frequency band for small events. While M_0 usually is estimated accurately by the available approaches, the other source parameters (e.g., corner frequency, and stress drop) frequently show considerable variability, suggesting that data and methods often are inadequate to constrain the dynamic features of the source (Kwiatek et al. 2014; Abercrombie 2015; Kaneko and Shearer 2015; Trugman and Shearer 2017).

To obtain a simple and fast estimation of the M_W for events with M ≤ 4, usually not available from the inversion of the time recordings, Atkinson et al. (2014) proposed a procedure that correlates the response spectra computed at fixed periods (i.e., 0.3 and 1.0 s) with the M_W values of the analyzed earthquakes. The advantage of using response spectra instead of Fourier amplitude spectra is that, being calculated by applying a 5% damping, they smooth the irregularities observed in the Fourier spectra. Moreover, the response spectra at 0.3 and 1.0 s are widely used engineering parameters that are often available in real time (e.g., ShakeMap parameters) and thus can be used to provide rapid estimates of M_W. Moratto et al. (2017) applied this method to the weak seismicity recorded in Northeastern Italy and observed underestimation of M_L with respect to M_W for earthquakes with $M_W < 1.5$. Similar results were obtained by Moratto et al. (2019), who inverted the full source spectra to estimate the seismic moment and the corner frequency for a selection of 30 well-located earthquakes with $1.0 ≤ M_L ≤ 3.0$ occurred in a restricted area of Northeastern Italy. Even though M_L-M_W discrepancies may be related to source and rupture complexities (Deichmann 2006), it has been recently proved that the main reason for which M_L underestimates the seismic energy released by microearthquakes (indicatively, for $M_L < 1.5$) is the fast decay of the high-frequency

amplitude due to the anelastic attenuation and scattering, which act as a low-pass filter on the recordings; so, for small events, the pulse durations become constant and the amplitudes (M_L) decrease strongly to balance the seismic moment. Consequently, the frequency-magnitude relationship based on M_L may result biased for low magnitudes (Deichmann 2017).

Since the end of the first decade of the 2000 years, the National Institute of Oceanography and Applied Geophysics (OGS) has been in charge of the seismic monitoring of the underground gas storage (UGS) activity managed by Edison Stoccaggio S.p.A. at Collalto, a small locality of Northeastern Italy (Fig. 1; Priolo et al. 2015). A dedicated seismic monitoring infrastructure, the Collalto Seismic Network (Rete Sismica di Collalto, RSC), was realized and is fully operating since January 1, 2012. As a result of this activity, a seismic catalog that consists of almost 2000 events to date has been produced and represents a unique opportunity to test and apply new methods for the analyses of the microseismicity. Being in a seismically active area, fast and reliable estimation of the main source parameters—primarily the magnitude—is needed.

In this work, we use and extend the method originally proposed by Atkinson et al. (2014) and applied by Moratto et al. (2017) to Northeastern Italy at regional scale, to estimate the moment magnitude of the microseismicity recorded by the RSC in the period 1 January 2012–31 July 2018. The ultimate goal is to have a robust and fast procedure for the quasi real-time estimation of M_W using the response spectra even for very small earthquakes.

2 The seismic monitoring of the Collalto UGS

2.1 The Montello-Collalto area

The Collalto UGS is situated in the Montello-Collalto area, at the outer front of the Southeastern Alps, in Northeastern Italy (Fig. 1). This sector of the Alpine chain belongs to the collision zone between Adria and Europa plates, which are approaching each other with a shortening rate of 1.5–2 mm/year (Cheloni et al. 2014).

The Montello-Collalto area belongs to the seismic district called Pedemontana Sud (in English, Southern Foothills), which was historically interested by a destructive M6+ earthquake in 1695, besides several other damaging events (Sugan and Peruzza 2011 and
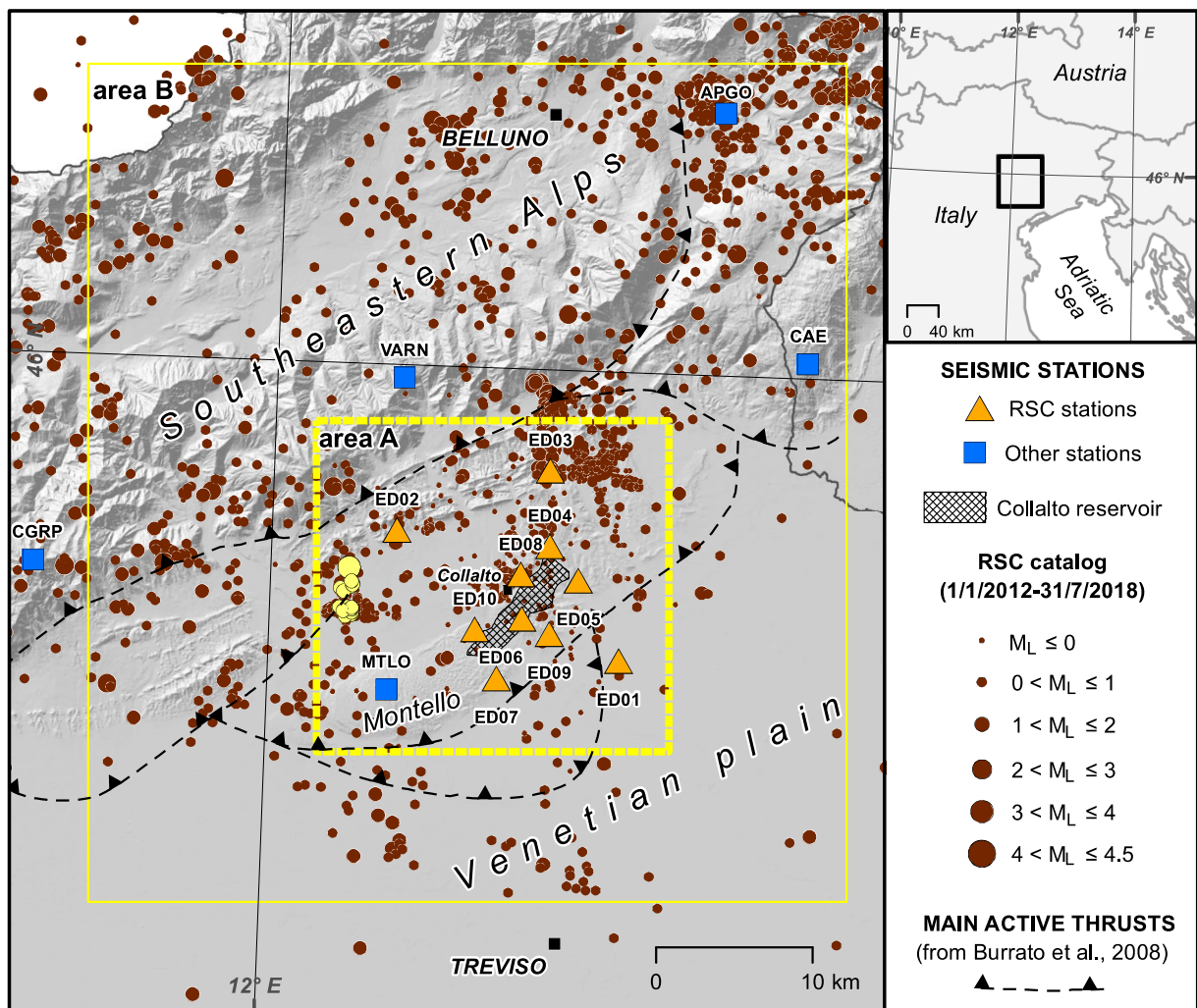
Fig. 1 Epicentral map of earthquakes recorded by the RSC in the period 1 January 2012–31 July 2018; the yellow rectangles represent area A and B. The yellow circles represent the 17 events belonging to the seismic sequence selected for the analysis shown in Fig 2

references therein). Although the seismicity located by the OGS regional network in recent years is weak (M ≤ 4; rts.crs.inogs.it, last accessed on August 2019), there are several evidences based on geomorphological, geodetic, and seismological observations that this area is tectonically active (Romano et al. 2019 and references therein).

The national seismic hazard map attributes to this area a medium-high hazard level, being characterized by values of horizontal peak ground acceleration on rock site of 0.20–0.25 g, with 10% exceedance probability in 50 years (Working Group MPS 2004). As the Montello-Collalto area is densely populated and site of several agricultural and industrial activities, the seismic

risk is relevant (Meroni et al. 2008) and particular care must be taken for any activity that is potentially able to accelerate the natural seismicity or induce earthquakes (Edwards 2015).

2.2 The Collalto UGS

The UGS activity developed at Collalto exploits a depleted natural gas reservoir located at the hanging wall anticline of the Montello thrust, one of the active faults accommodating the plate convergence in the area (Burrato et al. 2008; Cheloni et al. 2014; Fig. 1). The reservoir extends approximately over a 10 km × 4 km area at 1500-1600 m of depth. The UGS activity started

in 1994 and operates in a traditional way, i.e., the gas is injected into the reservoir during the warm season and is extracted from it during the cold one (Priolo et al. 2015). For more than 15 years, the gas storage pressure has been held within approximately the 80% of the pressure at which the gas was found within the reservoir (~ 160 bar). At the end of the first decade of the 2000 years, Edison Stoccaggio S.p.A. requested to increase the storage pressure to the original confining pressure, in order to expand the gas storage capacity. In 2011, the Italian Ministry for the Environment allowed the company to take this action but recommended that a seismic monitoring system able to detect earthquakes potentially induced by the storage activity had to be realized.

2.3 The Collalto Seismic Network

The RSC is a permanent high-resolution seismic network that was designed to detect and locate both microearthquakes potentially occurring nearby the reservoir (reference area A in Fig. 1) and strong events (M_W 5+) that can be released by the seismogenic faults existing in the surroundings (reference area B in Fig. 1; Burrato et al. 2008).

The local network is composed of a cluster of 7 stations deployed in the area above the reservoir with a mutual spacing of approximately 3–4 km and 3 more stations placed around at distance of approximately 10 km. The RSC network is complemented by approximately 30 additional stations of the regional seismic network managed by OGS within a ~ 80 km distance range. All the 10 RSC stations are equipped with high-sensitivity velocimeters; 1 station has a broad-band seismometer with natural period 120 s, while the other 9 stations have borehole seismometers with natural period ranging from 10 to 30 s. Five stations complement the velocimeters with high-dynamic accelerometers deployed at surface. Signals are sampled at 200 Hz (100 Hz for the accelerometers) and transmitted in real-time to the OGS acquisition center, where they are processed and archived permanently. An automatic system detects and locates the seismic events in real time. All detections are reviewed at a second time by a seismologist; at this level, all seismic events are validated and relocalized manually. More details can be found in Priolo et al. (2015) and Romano et al. (2019).

At present, the RSC is one of the few seismic networks devoted to monitoring a UGS activity in Italy for which data are public. Complete information about the RSC, as well as the reports and earthquake catalog updated on a 6-month basis, are freely available on the RSC website (see Section 6.1).

2.4 The RSC earthquake dataset

The seismic catalog used in this study covers the period 1 January 2012–31 July 2018 and contains 1773 events mainly located in the area represented in Fig. 1. Earthquake locations are obtained through a standard procedure that uses Hypo71 (Lee and Lahr 1975) with a regional 1D velocity model calibrated for the Northeastern Italy (Bressan et al. 2003), station delays to account for the elevation and the local heterogeneities of the velocity model, and constant V_P/V_S ratio equal to 1.78 as determined by the modified Wadati diagram.

The local magnitude M_L is estimated using the attenuation law obtained by Bragato and Tento (2005) for Northeastern Italy and applying statistical corrections to remove station static residuals. M_L varies from a minimum value of − 1.8 to a maximum of 4.5, but 98% of events has $M_L \leq 2$. So, the RSC earthquake dataset consists essentially of microearthquakes. The only event with $M_L > 4$ is located just outside the area B, and thus, it is of no interest for this study.

The main features of the microseismicity recognized by the RSC after 6 years of monitoring are documented in Moratto et al. (2019) and Romano et al. (2019). It appears entirely of tectonic origin, and no evidence has been found for any possible effect of the gas storage activity on the seismicity. In particular, all located seismicity occurs at distances larger than 3 km from the gas reservoir—we remind that the value of 3 km is assumed by the Italian Monitoring Guidelines as the maximum distance at which microseismicity may be induced by gas storage activity (MiSE 2014); no space-time correlation has been found between the storage activity and seismicity; no migration of earthquakes (over the completeness magnitude threshold) has been detected from the Collalto gas reservoir towards the surroundings; the hypocentral depth distribution is geometrically consistent with the active part of the Montello thrust, of which it provides a detailed portrait.

Despite the tectonic nature of RSC earthquakes, it is well known that the discrimination between natural and induced/triggered seismicity is neither a trivial matter nor has it been solved definitively (Grigoli et al. 2017). It relies on accurate and fast earthquake location

and source parameter estimation. Therefore, an effective procedure for M_W estimation of weak earthquakes in seismically active area where human activities are potentially able to induce earthquakes is crucial to interpret the origin of microseismicity and make seismic monitoring of underground industrial activities a more effective tool.

3 Extending the M_W evaluation to microseismicity

As already mentioned in Section 1, the original method for estimating M_W from the response spectra, M_W(SA), was proposed by Atkinson et al. (2014). In their study, they used the spectral ordinates calculated at periods of 1.0 (SA10) and 0.3 s (SA03) for estimating M_W in the range 3.0–4.0 and $M_W < 3.0$, respectively.

Later on, Moratto et al. (2017) applied the same approach to a set of 1823 earthquakes recorded in Northeastern Italy at regional scale and calibrated through the following relation:

$$\log(\text{SA}[T]) = a \times M_W + D(r, r_{\text{ref}}, f) + c_T, \qquad (1)$$

where a quantifies the magnitude scaling factor, $D(r, r_{\text{ref}}, f)$ represents the propagation term as a function of the hypocentral distance (r) and c_T is a constant defined specifically for the response spectra computed at various periods ($f = 1/T$). Moratto et al. (2017) estimated the scaling factor a equal to 1.49, observing that it is similar to the typical scaling of 3/2 (or reciprocally its inverse 2/3) between M_W and M_L. It has actually been demonstrated that the scaling coefficient between log (SA) and M_W is exactly 2/3, the principal reason being the anelastic attenuation, i.e., the same explanation for the 3/2 scaling between M_L and M_W observed for small earthquakes (Deichmann 2017; Moratto et al. 2017). In particular, the amplitude value of the response spectrum at a particular period is equivalent to measuring the maximum amplitude of a seismogram filtered with a narrow second-order pass-band filter with a certain amount of damping, independently of the seismic moment. Since the measured maximum amplitude scales 1:1 with seismic moment M_0, and given the relationship between M_W and $\log(M_0)$, the coefficient of proportionality between M_W and the logarithm of the maximum amplitude, and thus also $\log(\text{SA})$, must therefore be exactly 2/3.

We verify the above statement on a selected set of 17 earthquakes (yellow circles in Fig. 1), which belong to the same seismic sequence, so that we can assume that all signals have identical radiation pattern and propagation effects. We analyze only the vertical component signals recorded at ED10 station (Fig. 1). On one hand, we calculate SA03 and SA10 values. On the other hand, we filter them with a narrow band-pass between 1.0 and 4.0 Hz and evaluate the maximum velocity (V_M). It comes out that V_M scales 1:1 with the response spectra SA03 (Fig. 2a) and SA10 (Fig. 2b). Then, we calculate the moment magnitude of each event by applying the approach proposed by Deichmann (2017), i.e., as a relative measure to a reference earthquake of the same sequence for which M_W has been estimated independently. According to this method, the M_W of the generic earthquake is obtained by scaling M_W of the reference by a factor corresponding to the ratio of the two spectral plateau amplitudes. We take the event of May 15, 2015 at 05:35:46.95 UTC, as a reference earthquake, for which a moment magnitude $M_W = 3.5$ has been estimated by the moment tensor technique (Saraò 2016). Then, we calculate M_W for the remaining 16 earthquakes of the selected seismic sequence and compare them to SA03 and SA10 (Fig. 2c and d, respectively). It clearly comes out that M_W scales 2:3 with both SA03 and SA10. The validity of the adopted procedure is confirmed for a specific event, i.e., the $M_W = 2.2$ occurred on May 15, 2015 at 11:33:43.00 UTC. For this case, the M_W obtained by the Deichmann (2017) approach is comparable with the value computed independently by Moratto et al. (2019), who inverted the source spectra to estimate the moment magnitude.

So, the magnitude scaling factor may be held constant and equal to 2/3 for all periods of the response spectra considered in the M_W computation. Further, we adopt the propagation term, $D(r, r_{\text{ref}}, f)$, proposed by Malagnini et al. (2002) for Northeastern Italy where the reference distance r_{ref} is 40 km. The constants c_T are set at 5.38 for SA03 and 6.63 for SA10 (Moratto et al. 2017). For Northeastern Italy, the value of transition between the two magnitude ranges moves from 3.0 to 2.6, so that SA10 and SA03 values are used for $2.6 \leq M_W \leq 4.0$ and $M_W < 2.6$, respectively. In their study, Moratto et al. (2017) are able to estimate M_W for microearthquakes down to 0.6. However, it is clear that the signal-to-noise ratio (SNR) tends to decrease as events become smaller and smaller, and this makes it impractical to calculate the magnitude for an increasing number
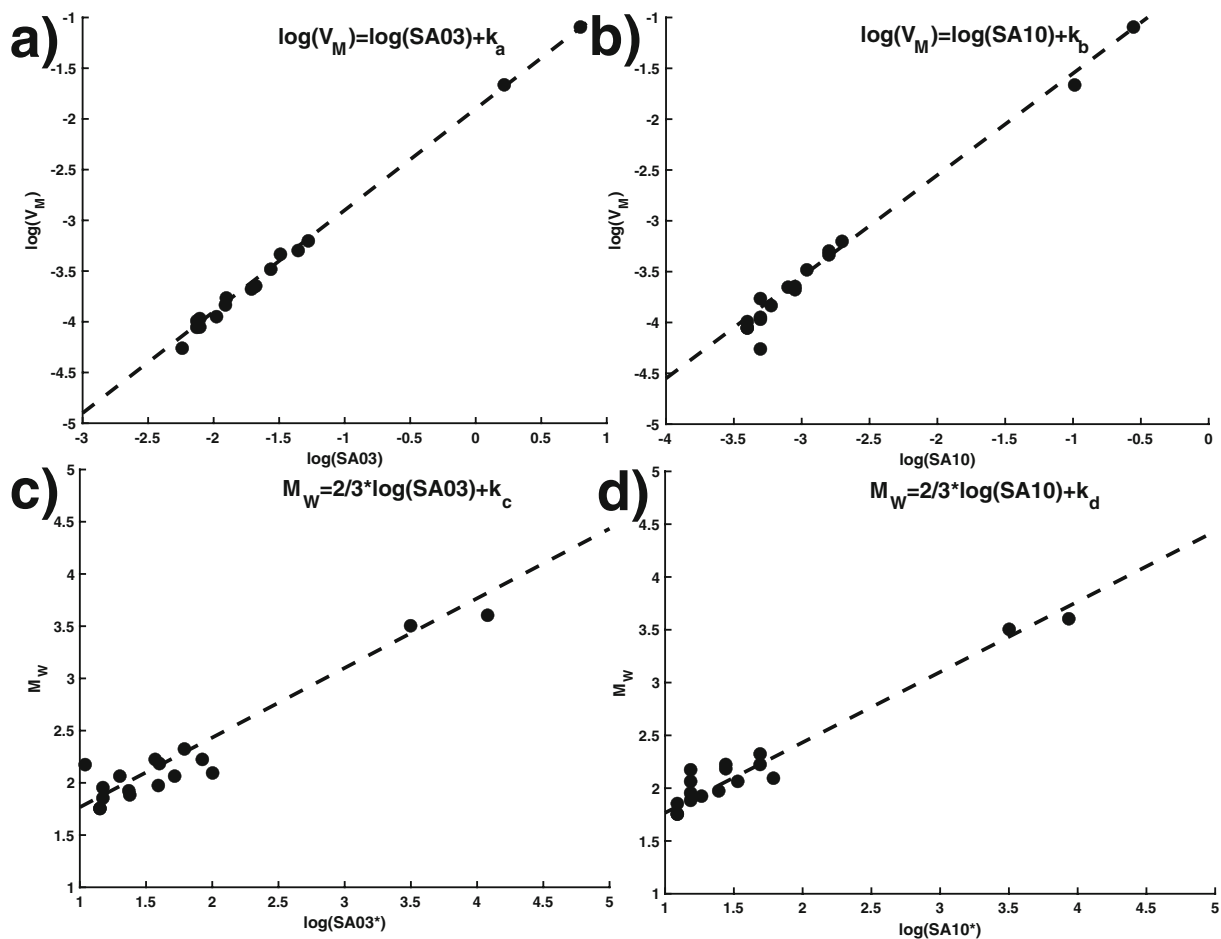
Fig. 2 **a** Comparisons between SA03 and V_M, **b** SA10 and V_M, **c** SA03 and M_W, and **d** SA10 and M_W for the seismic sequence of Fig. 1 (yellow circles); the dashed lines represent the fitting trend, which scales 1:1 above (**a**, **b**) and 2:3 below (**c**, **d**). In **c** and **d**, SA03 and SA10 data are normalized to the reference M_W values

of microevents as their size decreases. The SNR threshold is a critical parameter to choose, since a too low value would lead to estimate the magnitude of the noise, while a too high value would exclude many useful recorded data and leave M_W undefined for some earthquakes. The same authors suggest switching to lower periods (e.g., 0.2 or 0.1 s) to be more effective (i.e., to keep the SNR at a suitable level) in the low range of magnitudes. So, we investigate in this study the option of using spectral ordinates calculated at 0.1 s (SA01).

4 Calibration of the method for RSC

The $M_W(SA)$ algorithm requires a tuning of the working parameters for the study area in order to obtain reliable M_W estimations. This tuning concerns two different parts, i.e., the parameters that optimize the algorithm's execution and the coefficients that define the $M_W(SA01)$ correlation, respectively.

Concerning the first part, the following configuration parameters are evaluated: length of the earthquake signal to be analyzed, SNR threshold, and maximum station-event distance to be considered. Those parameters that maximized the number of events for which M_W is successfully estimated are considered optimal. Several sensitivity tests performed on a 1-month sample dataset demonstrate that the parameters used by Moratto et al. (2017) are suitable also for the RSC data, with only few changes. The following setting resulted eventually optimal for the RSC:

- Each record consists of 60 s of signal extracted from the vertical component, with 20 s of pre-event (i.e.,

before the P-wave arrival time) ambient noise included. This choice is for limiting the possibility to select signals containing more than one earthquake. Its value depends on the characteristics of the study area and the maximum source-receiver distance allowed.

- Minimum SNR threshold set at 3.0, with noise and signal time-window set at 0–15 s and 30–45 s, respectively. The latter is for isolating the main S-wave packet.
- Maximum hypocentral distance of 80 km, reduced to 40 km for earthquakes with $M_L < 1.5$, for the selected signals. This choice is for avoiding possible P- and S-wave contamination by secondary wave arrivals (e.g., the Moho reflections observed by Bragato et al. 2011).

Since all RSC seismometers are deployed mainly in shallow boreholes drilled in soft-to-stiff soils (Priolo et al. 2015), all signals have been corrected for the site response. As shown by Laurenzano et al. (2017), this step is crucial for the analysis of borehole records at the frequency band of our interest to remove the spectral effect (notches) produced by the interference of upgoing and downgoing body waves at depth and reproduce the free-surface bedrock conditions. The site responses for the RSC stations were those already estimated by Moratto et al. (2019) through the generalized inverse technique using a nearby bedrock station (i.e., VARN, Fig. 1) as a reference site. The amplification functions for the vertical component (Fig. 3) evidence well how the recorded signals are amplified by the local soil conditions at 1.0 s and 0.3 s. It can also be seen some notches in the high frequency band (around 0.1 s) that are related to the borehole installation and produce deamplification in some cases. These corrections are implemented through a spectral ratio between signal and site response spectrum. The adoption of the specific amplification curves shown in Fig. 3 improves greatly both the reliability and accuracy of the M_W estimations, as it comes out from the following test where we compare the $M_W(SA)$ estimated with and without considering the site effects to the M_W computed by Moratto et al. (2019) through the parametric approach of Zollo et al. (2014). The distribution of the residuals (Fig. 4) clearly shows that without the amplification curves, our procedure overestimates the moment magnitude by an average factor of 0.18 ± 0.09, while, applying the site effects, our $M_W(SA)$ estimation fits satisfactorily the values proposed by Moratto et al. (2019) and features a very low mean residual equal to 0.01 ± 0.06.

The second part of the tuning concerns the estimation of the coefficients of the relationship between SA01 and M_W. Moratto et al. (2017) showed that Eq. (1) holds for both SA10 and SA03; thus, we may assume that the same Eq. (1) holds also for SA01 and we focus on assessing the other equation coefficients. Considering that the attenuation term $D(r, 40, f)$ is that defined by Malagnini et al. (2002), the only coefficient to be estimated for tuning Eq. (1) for SA01 is c_T. This calibration must be done by fitting the $M_W(SA01)$ with $M_W(SA03)$ for earthquakes selected in a magnitude range where both SA01 and SA03 give reliable estimations, that is, in the range where the noise and the presence of the corner frequencies do not condition the final results. So, similarly to what is done in Atkinson et al. (2014) and Moratto et al. (2017), we compute numerical simulations for SA01 data using an approach based on point-source stochastic simulations (Boore 1983; Boore 2003). This method is based on the Band-Limited White Noise–Random Vibration Theory and considers a shear-wave amplitude spectrum as the product of filter functions that represent the source, site effects, and propagation path, which are modeled through geometrical spreading, anelastic attenuation, and ground-motion duration effects. The input parameters for the simulations were taken from Malagnini et al. (2002). The results of this analysis are shown in Fig. 5, which evidences how SA01 begins to saturate at $M_W = 2.0$ because the corner frequency limits the $M_W(SA)$ estimations (Moratto et al. 2017). Since we have seen that the relationship $M_W(SA03)$ holds for magnitude values down to less than 1.0, we calibrate the coefficient c_T by matching the values of M_W calculated separately using periods 0.3 and 0.1 s ($M_W(SA03)$ and $M_W(SA01)$, respectively) for all the events of the RSC catalog in the magnitude range 1.0–1.5, where we know that both relationships hold. The value resulting from this match is $c_T(SA01) = 4.46$, and the equations that define M_W for three periods are:

$$M_W(SA) = 2/3 \times (\log(SA10) - D(r, 40, 1.0) + 6.63) \quad (2)$$
$$\text{for } 2.6 \leq M_W \leq 4.0$$

$$M_W(SA) = 2/3 \times (\log(SA03) - D(r, 40, 3.3) + 5.38)$$
$$\text{for } 1.5 \leq M_W < 2.6 \quad (3)$$

$$M_W(SA) = 2/3 \times (\log(SA01) - D(r, 40, 10) + 4.46) \quad (4)$$
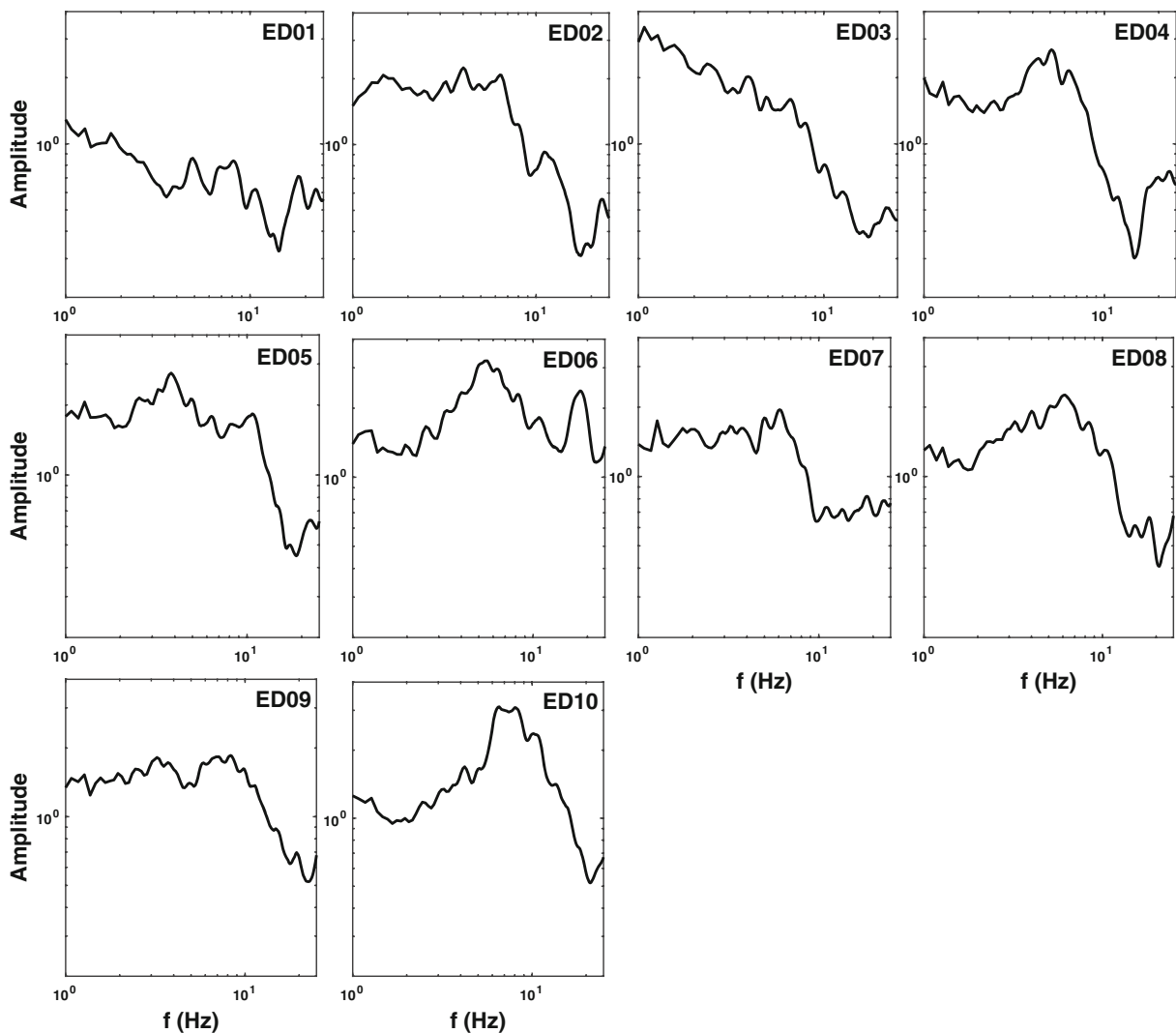$$\text{for } M_W < 1.5.$$

Fig. 3 Site response curves proposed by Moratto et al. (2019) for the vertical components of all the RSC stations

As a final step of the calibration process, we validate the new relationship M_W(SA01) with the numerical simulation of Fig. 5. It can be seen that the numerically simulated pseudo-spectral values at period 0.1 s fit accurately those estimated by the empirical relation (4) for the whole distance range considered for $M_W \leq 1.0$. The fit is less accurate but still good for $M_W = 2.0$, so that we can argue that Eq. (4) is effectively accurate for $M_W \leq 1.5$. Figure 5 also shows two different levels of ambient noise taken from Atkinson et al. (2014) from which we can appreciate the different limits in terms of station-event distance at which the proposed approach is able to estimate M_W in the presence of high or low seismic noise, respectively.

5 Results and discussion

Out of the 1773 events of the RSC catalog, with $-1.8 \leq M_L \leq 4.5$, the M_W is estimated successfully for 1381 events using the two periods originally proposed by Moratto et al. (2017), SA10 and SA03. This number increases to 1659, with a magnitude range $0.4 \leq M_W \leq 3.5$, when SA01 is added to the set of the periods used through Eq. (4). The new 278 events increase the percentage of success of the proposed procedure from ~ 78 to $\sim 94\%$ of the total RSC catalog; this improvement can be appreciated in Fig. 6, which compares the distributions of the M_W values computed applying the procedure proposed by Moratto et al. (2017) and the new

Fig. 4 Distributions of the residuals (with the related mean value) between the $M_W(SA)$ of this study and the M_W evaluated by Moratto et al. (2019) for a subset of 16 earthquakes. The picture compares $M_W(SA)$ values estimated either without considering any site effect (orange; mean value: dotted line) and those taking into account the specific amplification curves of Fig. 3 (blue; mean value: solid line)
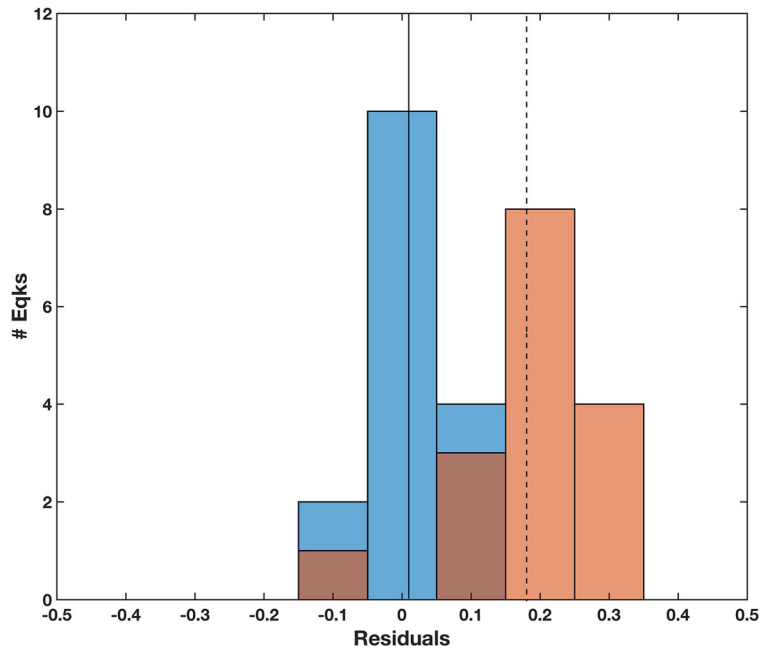
approach that uses the SA01 data. Note also that using 3 periods instead of 2 has much more effect in populating the low magnitude range instead of decreasing significantly the minimum estimated magnitude—we remind here that the lowest magnitude calculated by Moratto et al. (2017) was 0.6. Note also that most of the rejected earthquakes did not pass the SNR criterion because their waveforms contained the coda of larger events occurred just before them. A critical issue is that SA01 makes estimates less stable than SA10 and SA03, since the crustal heterogeneities at small length scale are cause of major scattering in the high frequency band.
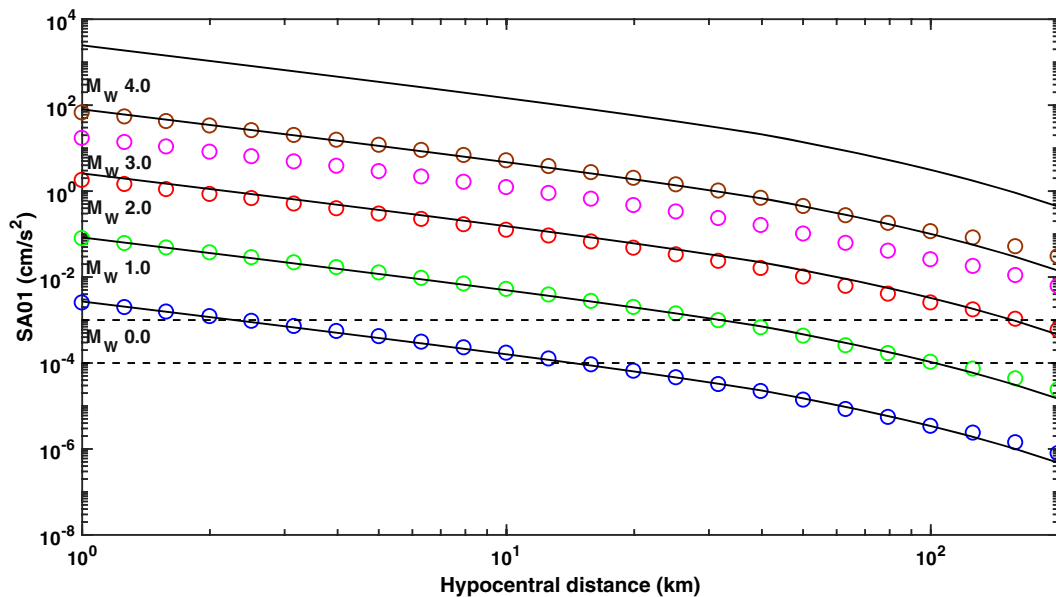

Fig. 5 Comparison between the pseudo-spectral values calculated at period 0.1 s (SA01) simulated numerically (empty circles) and estimated by Eq. (4) (continuous line). The diagram shows M_W as a function of the hypocentral distance (in kilometers). The horizontal dashed lines indicate the average standard values for the high (10^{-3} cm/s^2) and low (10^{-4} cm/s^2) noise level, according to Atkinson et al. (2014)

Fig. 6 M_W distributions with (blue) and without (orange) the SA01 data (Eq. 4)
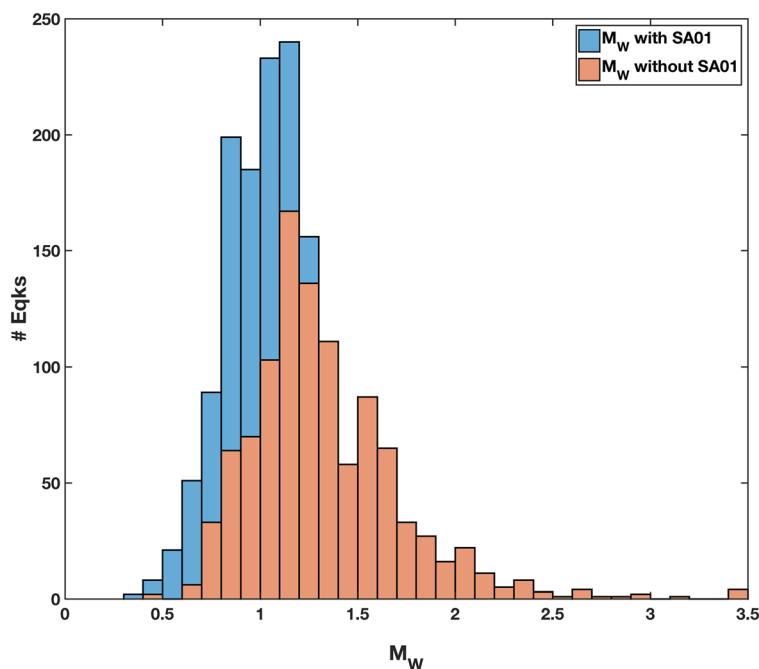
Therefore, the relative uncertainty associated to M_W increases from a mean of 0.09 for $M_W \geq 1.5$ to 0.17 for $M_W < 1.5$.

The pre-processing described in Section 4 can be considered as an improvement of the original approach proposed by Atkinson et al. (2014) and is part of the tuning stage. The results obtained in this study show that its application has increased both the number of events for which M_W has been calculated and the M_W accuracy.

Figure 7a compares M_W obtained in this study with M_L of the starting RSC catalog. M_W estimations tend to scatter as the magnitude decreases, as an effect of a loss of accuracy due to either low SNRs or less accurate hypocentral locations or major scattering influencing the SA01 data. An additional source of scatter of the Mw estimates from SA01 is the more irregular nature of the response spectra at periods around 0.1 s than at 0.3 and 1 s. Note that for $M_L < 2.5$, M_L and M_W deviate, being M_W systematically larger than M_L. Using an orthogonal regression, we estimate the following relationship between M_L and $M_W(SA)$:

$$M_W(SA) = 0.68(\pm 0.02) \times M_L + 0.82(\pm 0.04) \quad (5)$$

The scaling factor equal to 2/3 is predicted by the theory, which relates this trend observed in the M_W-M_L relation for small earthquakes to the effect of the anelastic attenuation that makes constant the pulse durations of the recorded signals (Deichmann 2017). Further, the resulting 2/3 coefficient confirms similar results obtained in other regions (e.g., Zollo et al. 2014; Munafò et al. 2016; Moratto et al. 2017). This optimal agreement with theoretical models and previous studies is an additional confirmation that $M_W(SA)$ is reliable for estimating the moment magnitude. Note also that the value of the additive constant varies from the 0.72 estimated for the Northeastern Italy by Moratto et al. (2017) to the 0.82 estimated for the area of Collalto in this study. While some authors associate it to the crustal attenuation of the studied area (Munafò et al. 2016), we cannot exclude that it may also be related to the procedure used to calculate M_L by the monitoring system.

Figure 7b shows the M_W station-residual as a function of the hypocentral distance. The average value range is ± 0.6. The residual distribution is quite stable for distances larger than 10–15 km, while the station-magnitude ($M_W(STA)$) tends to overestimate the event-magnitude ($M_W(EVT)$) at smaller distances, where unconsidered near-fault effects may become progressively more evident. Indeed, the largest negative residuals are associated with stations located just above the

Fig. 7 a Comparison between
M_L and Mw values computed in
this study for the RSC earthquake
dataset (epicentral map in Fig. 1).
b M_W station-residuals
(M_W(EVT)-M_W(STA)) as a function of the hypocentral distance
computed for each record
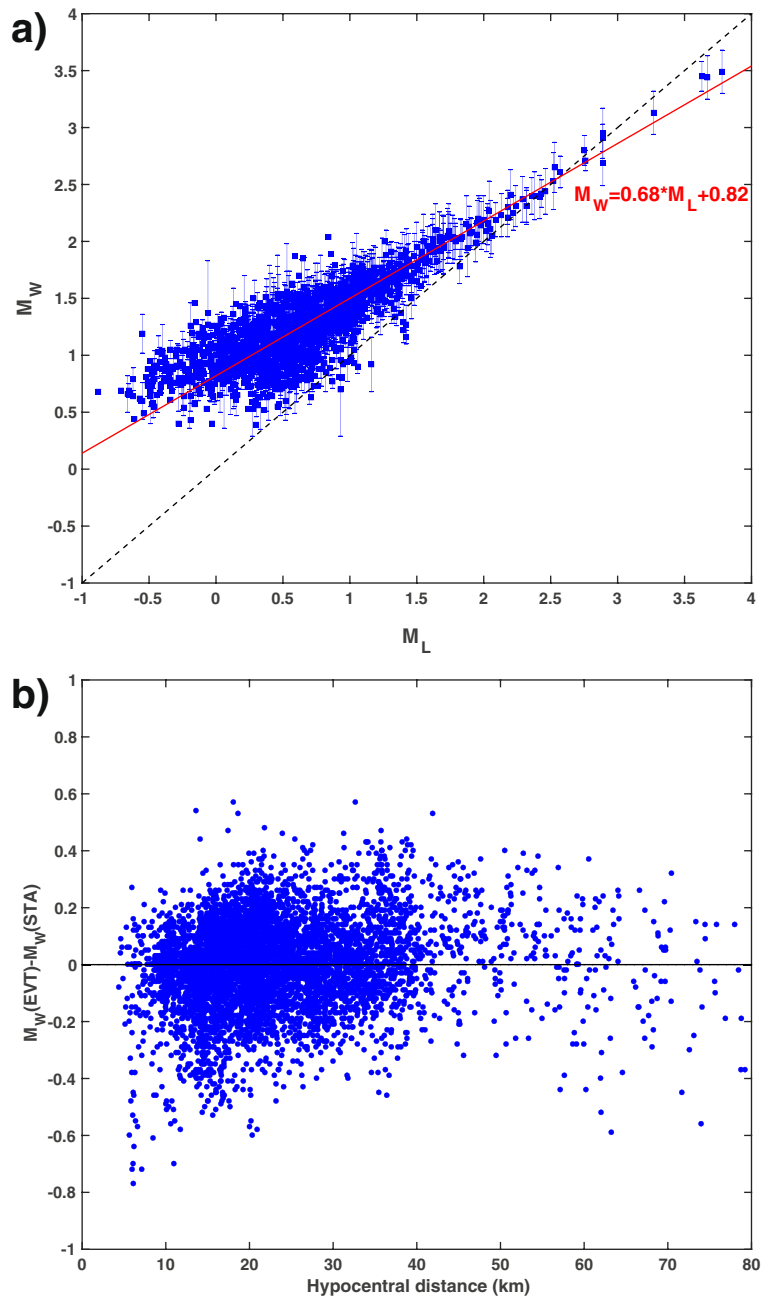
hypocenters, while our propagation model is calibrated for the far-field approximation. Another source of variability can also be related to some velocity anomalies in the source-receiver path compared to the average velocity model (Bommer et al. 2016). Further, the magnitude residuals are computed for each considered station (Table 1): we can notice that many stations have the mean residuals lower than ± 0.1 with the exception of

few stations potentially influenced by path propagation or soil effects where the residuals become 0.3. If we restrict our analysis to the EV stations only, the M_W station residuals range between -0.06 (ED10) and 0.04 (ED07) with the related standard deviations lower than 0.15.

We eventually estimate the completeness magnitude (M_C) and the Gutenberg-Richter parameters (a and b

Table 1 Magnitude residuals (the mean values with the related standard deviation) for all considered stations

Station	# data	Mean	Std. dev.	Station	# data	Mean	Std. dev.
ED01	62	− 0.04	0.14	CSM	23	0.11	0.12
ED02	377	− 0.05	0.14	CSO	310	0.11	0.12
ED03	536	0.00	0.12	CTI	137	− 0.05	0.14
ED04	417	0.01	0.10	DOSS	27	− 0.03	0.13
ED05	240	0.02	0.11	FAU	237	0.09	0.11
ED06	349	0.03	0.12	FUSE	9	0.11	0.08
ED07	245	0.04	0.10	IESO	2	− 0.36	0.11
ED08	509	− 0.03	0.12	MARN	19	− 0.05	0.13
ED09	226	0.03	0.09	MLN	257	0.12	0.13
ED10	422	− 0.06	0.11	MPRI	16	0.10	0.12
AFL	15	0.06	0.13	MTLO	422	− 0.15	0.15
AGOR	132	0.03	0.14	PANI	24	0.06	0.12
APGO	60	− 0.32	0.23	STAL	3	0.20	0.17
CAE	486	0.00	0.19	TEOL	15	− 0.23	0.11
CGRP	270	0.09	0.14	VARN	791	− 0.03	0.15
CIMO	320	0.06	0.15	ZIAN	32	− 0.11	0.12
CLUD	17	0.13	0.15	Total	7008	0.00	0.15

values) for the new M_W dataset and investigate how they change when using M_W instead of M_L. To this aim, we use the maximum-curvature and maximum-likelihood methods implemented in ZMAP software (Woessner and Wiemer 2005) for calculating M_C and parameters a and b, respectively. Figure 8 shows the frequency-magnitude relationships for M_L and M_W. The obtained M_C, annual a value, and b value are, respectively, 0.6, 2.7, and 0.9 for M_L (Fig. 8a) and 1.2, 3.6, and 1.2 for M_W (Fig. 8b). The bias in the values obtained for the two magnitudes derives directly from the noticeable bias in the distribution of the values (triangles in the diagrams of Fig. 8), being that obtained for M_L (with range from − 0.9 to 3.8) wider than that for M_W (with range from 0.4 to 3.5). As already mentioned, such a difference in the distributions is due to the deviation of M_W from M_L, which increases linearly as the magnitudes decrease for weak earthquakes (Ross et al. 2016).

Specifically, note that the b value changes from a value < 1 for M_L to a value > 1 for M_W, according to what already observed by Deichmann (2017). This result is very important, and it has to be taken into account when the b value, or its variation, are analyzed. For example, it is known that the b value is a crucial parameter for seismic hazard assessment (Cornell 1968;

Weichert 1980); it represents the relative number of large and small earthquakes in a specific area, and together with the a value, it is useful to provide an estimate of the maximum expected magnitude. However, it has been found that seismic hazard assessments based on M_L of small earthquakes likely overestimate the occurrence probability of large earthquakes (Staudenmaier et al. 2018). Another application is the discrimination between induced and natural seismicity, where b value deviations from its theoretical value may be symptomatic of induced seismicity (e.g., Stabile et al. 2014; Goebel et al. 2016).

6 Conclusions

Fast methods to calculate M_W are highly desirable, as this kind of magnitude provides an accurate estimation of the actual seismic energy released during an earthquake, especially for weak events (Moratto et al. 2017). In this study, we have estimated M_W for the microseismicity located by the RSC in more than 6 years of monitoring (period 1 January 2012–31 July 2018) in the tectonically active area of Montello-Collalto (Northeastern Italy). We have applied the approach proposed by Atkinson et al. (2014) based on the use of response spectra that scale 2/3 with M_W; we verify this relationship analyzing the vertical data recorded on a specific station for a seismic sequence occurred in 2015 in the monitored area. Our procedure, calibrated by Moratto et al. (2017) for Northeastern Italy, was improved in order to make it more effective for the M_W estimation of microevents (M_W < 1.5). In particular, we have extended the original approach by the use of an additional shorter period SA01 (0.1 s); despite the fact that M_W values derived from the SA01 data are affected by larger uncertainty, this development allows us to estimate the moment magnitude down to a minimum threshold of 0.4. Furthermore, we have introduced the site response correction within the calculation, to get rid of local site effects and the spectral distortion due to the deployment at depth of borehole velocimeters. The inclusion of specific site effects improves the final results significantly, as evidenced by the comparison with the moment magnitudes estimated by Moratto et al. (2019).

Using the new approach, we estimated M_W for 1659 out of the 1773 earthquakes present in the original catalog, with a 94% success percentage. The range of
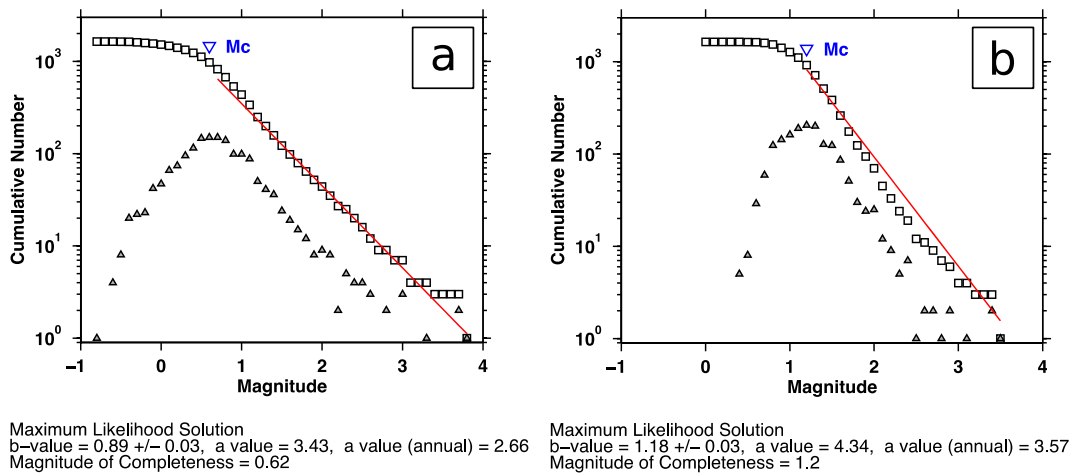
Fig. 8 Gutenberg-Richter cumulative (squares) and incremental (triangles) magnitude-frequency distributions (bin size 0.1) and completeness magnitude (M_C) estimated for the M_L (**a**) and M_W (**b**) datasets, respectively

the estimated magnitudes changes from the original $-0.8 \leq M_L \leq 3.8$ into $0.4 \leq M_W \leq 3.5$.

After orthogonal regression, M_W and M_L scales as 2/3, similarly to what observed in other areas, but with a slightly greater value of the additive constant (0.83) than that calculated by Moratto et al. (2017) for Northeastern Italy. The slight difference may be related either to different attenuation properties, considering the higher frequency band and shorter distance range of the data in this study, or to some discrepancies in the procedures implemented by the RSC and OGS Northeastern Italy seismic networks to estimate M_L. In any case, the 2/3 scaling factor agrees with the value predicted by the theoretical models and observed in previous studies and underscores the effectiveness of our procedure to estimate M_W values from the SA. The station-magnitude residuals remain quite constant except for hypocentral distances < 10 km, where near-fault effects (not considered here) may have more impact.

We have eventually estimated the frequency-magnitude relationship to assess the completeness magnitude (M_C) and the Gutenberg-Richter parameters (*a* and *b* values) for the new M_W dataset and compared the results obtained here to those based on M_L. Since M_L provides inconsistent estimates of the earthquake size when applied to either microseismicity or stronger earthquakes (Deichmann 2018), we recommend to evaluate the Gutenberg-Richter *a* and *b* parameters, as well as the magnitude of completeness, exclusively on the base of the frequency-M_W relationship. A more reliable *b* value is also important for discriminating between induced and natural seismicity, since it has been shown that its

variation could indicate the occurrence of induced seismicity (Stabile et al. 2014; Goebel et al. 2016).

This study demonstrates the effectiveness of the proposed method for quickly computing the M_W for microearthquakes. Our procedure is suitable to be implemented directly within standard routine analyses of real-time monitoring of underground industrial activities potentially capable to trigger seismicity in active tectonic regions, in order to interpret the origin of microseismicity better and feed decision-making processes (e.g., the traffic light protocols).

6.1 Data and resources

The Collalto Seismic Network (Rete Sismica di Collalto - RSC, doi:10.7914/SN/EV) is managed by the National Institute of Oceanography and Applied Geophysics (OGS) on behalf of Edison Stoccaggio S.p.A.

The RSC data are freely available from the OGS Archive System of Instrumental Seismology (OASIS, http://oasis.crs.inogs.it/); RSC also uses data from the Northeastern Italy Integrated Seismic Network (NEI, doi.org/10.7914/SN/OX, managed by the OGS on behalf of the Veneto Region and the Autonomous Region of Friuli Venezia Giulia) and data from some networks with codes ST, NI, and IV registered at the FDSN (International Federation of Digital Seismograph Networks, http://www.fdsn.org/).

The earthquake catalog used in this study is available at the web site of the RSC - Collalto Seismic Network (http://rete-collalto.crs.inogs.it).

The following software systems were used: Antelope, developed by BRTT (http://www.brtt.com/); GMT - Generic Mapping Tools (http://gmt.soest.hawaii.edu/); ArcMAP developed by ESRI (http://desktop.arcgis.com/en/arcmap/); and ZMAP (http://www.seismo.ethz.ch/en/research-and-teaching/products-software/software/ZMAP/). All these websites were last accessed on August 2019.

References

Abercrombie RE (2015) Investigating uncertainties in empirical Green's function analysis earthquake source parameters. J Geophys Res 120:4263–4277

Atkinson GM, Greig WD, Yenier E (2014) Estimation of moment magnitude (M) for small events (M < 4) on local networks. Seismol Res Lett 85:1116–1124

Bommer JJ, Dost B, Edwards B, Stafford PJ, van Elk J, Doornhof D, Ntinalexis M (2016) Developing an application-specific ground-motion model for induced seismicity. Bull Seismol Soc Am 106:158–173

Boore D (1983) Stochastic simulation of high-frequency ground motions based on seismological models of the radiated spectra. Bull Seismol Soc Am 73:1865–1894

Boore D (2003) Prediction of ground motion using the stochastic method. Pure Appl Geophys 160:635–676

Bragato PL, Tento A (2005) Local magnitude in northeastern Italy. Bull Seismol Soc Am 95:579–591

Bragato PL, Sugan M, Augliera P, Massa M, Vuan A, Saraò A (2011) Moho reflection effects in the Po plain (Northern Italy) observed from instrumental and intensity data. Bull Seismol Soc Am 101:2142–2152

Bressan G, Bragato PL, Venturini C (2003) Stress and strain tensors based on focal mechanisms in the seismotectonic framework of the Friuli–Venezia Giulia region (Northeastern Italy). Bull Seismol Soc Am 93:1280–1297

Burrato P, Poli ME, Vannoli P, Zanferrari A, Basili R, Galadini F (2008) Sources of Mw 5+ earthquakes in northeastern Italy and western Slovenia: an updated view based on geological and seismological evidence. Tectonophysics 453:157–176

Cheloni D, D'Agostino N, Selavggi G (2014) Interseismic coupling, seismic potential, and earthquake recurrence on the southern front of the Eastern Alps (NE Italy). J Geophys Res Solid Earth 119. https://doi.org/10.1002/2014JB010954

Cornell CA (1968) Engineering seismic risk analysis. Bull Seismol Soc Am 58:1583–1606

Deichmann N (2006) Local magnitude, a moment revisited. Bull Seismol Soc Am 96:1267–1277

Deichmann N (2017) Theoretical basis for the observed break in M_L/M_w scaling between small and large earthquakes. Bull Seismol Soc Am 107:505–520

Deichmann N (2018) The relation between M_E, M_L and M_w in theory and numerical simulations for small to moderate earthquakes. J Seismol 22:1645–1668

Dreger DS (2002) TDMT_INV: Time-domain seismic moment tensor inversion. In: Lee WHK, Kanamori H, Jennings PC, Kisslinger C (eds) International handbook of earthquake and engineering seismology, vol 81B. Academic Press, Amsterdam 1627p

Dziewonski AM, Chou TA, Woodhouse JH (1981) Determination of earthquake source parameters from waveform data for studies of global and regional seismicity. J Geophys Res 86:2825–2852

Edwards B (2015) The influence of earthquake magnitude on hazard related to induced seimicity. In: Ansal A (ed) Perspectives on European Earthquake Engineering and Seismology, Geotechnical, Geological and Earthquake Engineering 39. https://doi.org/10.1007/978-3-319-16964-4_18

Goebel THW, Hosseini SM, Cappa F, Hauksson E, Ampuero JP, Aminzadeh F, Saleeby JB (2016) Wastewater disposal and earthquake swarm activity at the southern end of the Central Valley, California. Geophys Res Lett 43:1092–1099

Grigoli F, Cesca S, Priolo E, Rinaldi AP, Clinton JF, Stabile TA, Dost B, Fernandez MG, Wiemer S, Dahm T (2017) Current challenges in monitoring, discrimination, and management of induced seismicity related to underground industrial activities: a European perspective. Rev Geophys 55. https://doi.org/10.1002/2016RG000542

Hanks TC, Kanamori H (1979) A moment magnitude scale. J Geophys Res 84:2348–2350

Kaneko Y, Shearer PM (2015) Variability of seismic source spectra, estimated stress drop, and radiated energy, derived from cohesive-zone models of symmetrical and asymmetrical circular and elliptical ruptures. J Geophys Res Solid Earth 120. https://doi.org/10.1002/2014JB011642

Kwiatek G, Bulut F, Bohnhoff M, Dresen G (2014) High-resolution analysis of seismicity induced at Berlín geothermal field, El Salvador. Geothermics 52:98–111

Laurenzano G, Priolo E, Mucciarelli M, Martelli L, Romanelli M (2017) Site response estimation at Mirandola by virtual reference station (2017). Bull Earthq Eng 15:2393–2409

Lee WHK, Lahr JC (1975) HYP071 (Revised): a computer program for determining hypocenter, magnitude and first-motion pattern of local earthquakes. US Geological Survey Open File Report 75-311. https://doi.org/10.3133/ofr75311

Malagnini L, Akinci A, Herrmann RB, Pino NA, Scognamiglio L (2002) Characteristics of the ground motion in northeastern Italy. Bull Seismol Soc Am 92:2186–2204

Meroni F, Pessina V, Bernardini A (2008) Damage risk and scenarios in the Veneto – Friuli area (NE Italy). Boll Geofis Teor Appl 49:485–504

MiSE (2014) Guidelines for monitoring seismicity, ground deformation and pore pressure in subsurface industrial activities. English version available at https://unmig.mise.gov.it/images/docs/151_238.pdf. Last accessed August 2019.

Moratto L, Saraò A, Priolo E (2017) Moment magnitude (M_W) estimation of weak seismicity in Northeastern Italy. Seismol Res Lett 88:1455–1464

Moratto L, Romano MA, Laurenzano G, Colombelli S, Priolo E, Zollo A, Saraò A, Picozzi M (2019) Source parameter analysis of microearthquakes recorded around the underground gas storage in the Montello-Collalto Area (Southeastern Alps, Italy). Tectonophysics 762:159–168

Munafò I, Malagnini L, Chiaraluce L (2016) On the relations between MW and ML for small earthquakes. Bull Seismol Soc Am 106:2402–2408

Priolo E, Romanelli M, Plasencia Linares MP, Garbin M, Peruzza L, Romano MA, Marotta P, Bernardi P, Moratto L, Zuliani D, Fabris P (2015) Seismic monitoring of an underground natural gas storage facility: the Collalto Seismic Network. Seismol Res Lett 86:109–123

Romano MA, Peruzza L, Garbin M, Priolo E, Picotti V (2019) Microseismic portrait of the Montello thrust (Southeastern Alps, Italy) from a dense, high-quality seismic network. Seismol Res Lett 90:1502–1517

Ross ZE, Ben-Zion Y, White MC, Vernon FL (2016) Analysis of earthquake body wave spectra for potency and magnitude values: implications for magnitude scaling relations. Geophys J Int 207:1158–1164

Saraò A (2016) On line catalogue of moment tensor solutions of earthquakes occurred in NE Italy and its surroundings in the period 2014–2016, available at http://bit.ly/2jlxfvv (last accessed August 2019)

Sipkin SA (1982) Estimation of earthquakes source parameters by the inversion of waveform data: synthetic waveforms. Phys Earth Planet Inter 30:242–259

Stabile TA, Giocoli A, Lapenna V, Perrone A, Piscitelli S, Telesca L (2014) Evidence of low-magnitude continued reservoir-induced seismicity associated with the Pertusillo artificial lake (Southern Italy). Bull Seismol Soc Am 104:1820–1828

Staudenmaier N, Tormann T, Edwards B, Deichmann N, Wiemer S (2018) Bilinearity in the Gutenberg-Richter relation based on M_L for magnitudes above and below 2, from systematic magnitude assessments in Parkfield (California). Geophys Res Lett 45:6887–6897

Sugan M, Peruzza L (2011) Distretti sismici del Veneto. Boll Geofis Teor Appl Supplement s3–s90, ISSN: 0006-6729

Trugman DT, Shearer PM (2017) Application of an improved spectral decomposition method to examine earthquake source scaling in Southern California. J Geophys Res Solid Earth 122:2890–2910

Weichert DH (1980) Estimation of the earthquake recurrence parameters for unequal observation periods for different magnitudes. Bull Seismol Soc Am 70:1337–1346

Woessner J, Wiemer S (2005) Assessing the quality of earthquake catalogs: estimating the magnitude of completeness and its uncertainty. Bull Seismol Soc Am 95:684–698

Working Group MPS (2004) Redazione della mappa di pericolosità sismica prevista dall'Ordinanza PCM 3274 del 20 marzo 2003, Rapporto conclusivo per il Dipartimento di Protezione Civile, Istituto Nazionale di Geofisica e Vulcanologia (INGV), Milano–Roma, aprile 2004, 65 pp. + 5 appendici (in Italian), http://zonesismiche.mi.ingv.it/documenti/rapporto_conclusivo.pdf. Last accessed August 2019

Zollo A, Orefice A, Convertito V (2014) Source parameter scaling and radiation efficiency of microearthquakes along the Irpinia fault zone in southern Apennines, Italy. J Geophys Res 119:3256–3275